ACS APPLIED MATERIALS & INTERFACES

Research Article

www.acsami.org

Spray Pyrolysis of $CuIn(S,Se)_2$ Solar Cells with 5.9% Efficiency: A Method to Prevent Mo Oxidation in Ambient Atmosphere

John C. W. Ho,[†] Tianliang Zhang,[‡] Kian Keat Lee,[‡] Sudip K. Batabyal,[‡] Alfred I. Y. Tok,[†] and Lydia H. Wong*[,†]

[†]School of Materials Science & Engineering, Nanyang Technological University, Singapore 639798

[‡]Energy Research Institute @ NTU, Nanyang Technological University, Research Techno Plaza, Singapore 637553

Supporting Information

ABSTRACT: Direct spray pyrolysis to form $CuInS_2$ (CIS) on molybdenum substrate in ambient environment has been a challenge because of the ease of Mo oxidation at low temperatures. MoO_2 formation affects the wettability of precursor solution during spray pyrolysis, which degrades the uniformity of CIS film and acts as a resistive layer for carrier transport. In this paper, Mo oxidation was prevented by using excess sulfur in the precursor solution under a gradual heating and spray process. A thin precursor layer was initially deposited as a barrier layer to prevent oxygen adsorption on Mo surface before the temperature was increased further to form polycrystalline $CuInS_2$. The $CuIn(S,Se)_2$ (CISSe) device fabricated from selenization of the spray-pyrolyzed CIS film exhibited a power conversion efficiency (PCE) of 5.9%. The simple spray method proposed here can be used to deposit a variety of Cu-based chalcopyrite precursor to produce high-quality thin film solar cells.

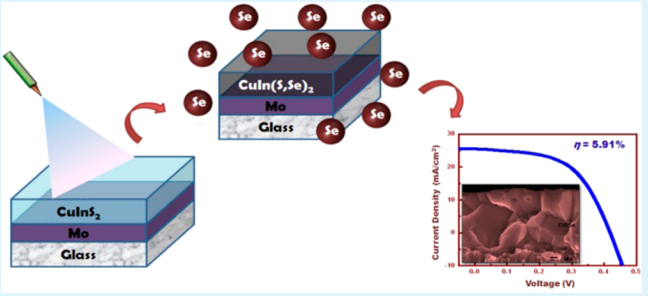

KEYWORDS: *spray pyrolysis, $CuInS_2$, $CuIn(S,Se)_2$, oxidation, photovoltaic, selenization, CIGS*

INTRODUCTION

Among the various materials for thin film photovoltaic (TFPV) applications in the market, $Cu(In,Ga)(S,Se)_2$ (CIGS) is an excellent absorber material, because of its tunable direct bandgap and high absorption coefficient. There are two main approaches for CIGS device fabrication namely vacuum and non-vacuum approaches. State-of-the-art CIGS thin film devices are fabricated under high vacuum conditions[1] and have achieved remarkable power conversion efficiency (PCE) in excess of 20%.[2] However, as the price of silicon is decreasing, research has focused on non-vacuum deposition of CIGS to reduce cost. Among the non-vacuum approaches, the use of hydrazine to dissolve binary-compound precursors (e.g., Cu_2S, In_2Se_3, and Ga_2Se_3) followed by spin coating of the mixture has been reported to yield high PCE of 15.2%.[3] Although the use of hydrazine has yielded high efficiency, its toxic and highly explosive nature poses environmental and manufacturing issues.

Other non-vacuum approaches such as nanoparticle or nano-ink approaches have also produced decent performances.[4−10] In the case of direct solution coating process, lower film purity due to residual impurities (e.g., C, O, and Cl) becomes the main hurdle in the device efficiency optimization.[11,12] Direct coating of solution precursor approach using organic solvent has been reported to result in thick carbon residue layer[13] or carbon impurities within the absorber film.[14−16] High-temperature Ar anneal followed by multistep selenization was able to remove ligands and achieved PCE of 7.1%.[17] The origin of the carbon impurities could be traced to the solvent or other binder materials. Carbon containing devices[13,14,16] typically showed a lower open-circuit voltage (V_{oc}) and fill factor (FF) as well as higher series resistances (R_s) as compared to carbon-free devices prepared by hydrazine approach.[3,18,19] Although there is exception in which such a thick carbon layer has been reported to have minimal impact on series resistance,[13] the general consensus is to avoid any carbon impurities to achieve optimum PCE.

Among the different solution-based techniques, spray pyrolysis has the potential for low-cost deposition.[20] Spray pyrolysis of $CuInSe_2$ thin film was successfully performed on glass substrates[21,22] and the corresponding devices prepared on indium tin oxide (ITO) substrate demonstrated PCE of 2%.[23] The ITO-based devices typically have low PCEs because of their higher resistivity, lower reflectivity, and less compatible work function. Furthermore, ITO is unstable during selenization. Finding alternative back contact materials with low resistivity and better work function compatibility to substitute ITO was deemed necessary. The compatibility of the work function of the back contact with that of the absorber material is important to reduce back contact recombination. In addition, the back contact material should have minimum reactivity with

Received: January 16, 2014
Accepted: April 3, 2014
Published: April 3, 2014

   dx.doi.org/10.1021/am500317m | ACS Appl. Mater. Interfaces 2014, 6, 6638−6643

both absorber layer and Se vapor during processing. The high reflectivity of back contact is also beneficial to reflect the unabsorbed light back into the absorber layer. Molybdenum (Mo) fulfills those criteria and demonstrates high PCEs when used as back contacts in chalcopyrite-based TFPV devices.

However, the susceptibility of Mo to oxidize at $T \geq 200°C$ tends to limit its applications to processes with stringent control of temperature and ambient gases. As such, Mo substrates are not often used for TFPV prepared via conventional spray pyrolysis. A rapid formation of thin molybdenum oxide layer is typically observed on the preheated substrates prior to the actual spraying process. The oxide layer reduces charge carrier collection efficiency due to its high resistivity and it may also affect the adhesion of the subsequent film. Oxidation can be prevented mainly by performing spray pyrolysis in an inert environment (e.g., N_2 glove box).[24] Unfortunately, excessive release of water vapor and other gases during the deposition may significantly impair the usability of the glove box in the long run. The option of lowering the preheating temperature is also not feasible as the threshold oxidation temperature of Mo is lower than the conversion temperature of the precursors to $CuInS_2$.

Here, we demonstrated successful spray pyrolysis of carbon-free CIS thin film on Mo-coated soda lime glass substrate without the formation of MoO_2 in an ambient environment. A gradual heating and spray process starting from low temperatures of 120 to 300−350 °C was employed to prevent any oxidation on Mo substrate. The atypical choice of the lower initial temperature is crucial as Mo oxidation occurs mainly in the early stages of the deposition. The gradual heating and spray process allows the formation of a thin layer of precursor materials and CIS film that can protect Mo surface from oxidation. In addition, the excess sulfur in the precursor mixture would induce preferential formation of MoS_2 instead of MoO_2. Selenization of MoS_2 resulted in $MoSe_2$ that causes minimal impact on both interface properties and band alignment at the back interface. Deionized (DI) water was also used as solvent instead of organic solvent to prevent residual carbon formation in the film. Spraying rate needs to be carefully controlled to allow sufficient time for chlorine (Cl) to escape in the form of HCl. No carbon, oxygen, or chlorine were detected in the final CISSe film as revealed by energy-dispersive X-ray spectroscopy (EDS) (detection limit ∼0.1 wt %). The photovoltaic device (glass/Mo/CISSe/CdS/ZnO/ITO/Al) made from selenized CIS thin film gave a PCE of 5.9%.

EXPERIMENTAL SECTION

Chemicals. The chemicals used are 99.99% copper(II) chloride hydrate ($CuCl_2{\cdot}nH_20$) and 99.99% indium chloride hydrate ($InCl_3.nH_2O$) purchased from Alfa Aesar and Thiourea ($SC(NH_2)_2$) purchased from Sigma-Aldrich.

Copper(II) chloride hydrate ($CuCl_2{\cdot}nH_20$, $n \approx 2$), indium(III) chloride ($InCl_3$) and thiourea $SC(NH_2)_2$ were dissolved in deionized (DI) water to form individual stock solutions.

Fabrication of CISSe Device. *Deposition of CIS Absorber Layer via Spray Pyrolysis.* To avoid the use of KCN etching of highly conducting secondary phases Cu_xSe or Cu_xS, the spray-pyrolyzed CIS film has to be Cu poor. Precursor solution was prepared with the overall goal of Cu poor absorber layer. Two precursor solutions were prepared by extracting from 0.1 M $CuCl_2$, 0.1 M $InCl_3$, and 1.0 M thiourea stock solutions. The first solution was Cu-rich and the second solution was Cu-poor. The Cu-rich layer aims to assist in the formation of intermediate CuS phase to assist grain growth during selenization, which was reported previously.[25] The Cu-poor solution was used to adjust the final Cu/In ratio of CIS film to be in the range of 0.75−0.9 to prevent formation of Cu_2Se after selenization, which is detrimental to device performance. Excess sulfur was added to the precursor solution. It should be noted that when the dispersion solution lacked of Sulfur, it resulted in the formation of a white precipitate, believed to be Cu-thiourea complex.[26] The dispersion containing the white precipitates is viscous and difficult to spray. The solution with excess sulfur was spray-deposited on Mo-coated glass substrates with N_2 as the carrier gas. A low initial substrate temperature of 120°C was chosen to prevent initial formation of molybdenum oxide. The temperature was ramped up concurrently with the spray process (Cu-rich precursor solution followed by Cu-poor precursor solution) with the final temperature at 300−350°C. The spraying rate can be tuned according to substrate temperature for better film thickness uniformity. Once the spray deposition was completed, the substrates were left to cool down naturally in ambient condition. As a control experiment, a spray pyrolysis process was also conducted with the substrate preheated to 300−350°C prior to the start of spray pyrolysis of precursor solutions. The deposited thickness was in range of 600−800 nm.

Annealing of CIS Absorber Film. The selenization of the spray-deposited film was done in an in-house tube furnace in Ar atmosphere. The CIS/Mo/glass samples were heat treated at 480−500°C in the presence of Se vapor in the tube. The gas flow within the tube furnace was regulated with inert Ar gas. The samples were allowed to cool naturally in the tube furnace at the end of selenization process.

Deposition of CdS, i-ZnO, ITO, and Al. The final devices were obtained after sequential deposition of CdS buffer layer, transparent conductive oxide (TCO) and electrode on the selenized CISSe films. CdS was deposited by chemical bath deposition (CBD) method, i-ZnO and ITO were deposited by DC sputtering while Al electrode by thermal evaporation.

Characterization. The spray-deposited samples were cleaved prior to cross-section analysis under a field-emission scanning electron microscope (FESEM), JEOL JSM-7600F. The cleaved sample was first coated with a thin Pt layer to prevent any charging effects. The film purity and Cu/In ratio were determined by an energy-dispersive X-ray (EDX) spectrometer at an accelerating voltage of 20 kV. As the K lines of sulfur and L lines of molybdenum are too close to resolve by EDX, analyses of overall film stoichiometry were conducted by wave dispersive spectroscopy (WDS) using the JXA-8530F field emission gun electron probe X-ray micro-analyzer (FEG-EPMA). Replicate point analyses were performed with a 5 μm defocused beam at a beam current of 20 nA and an accelerating voltage of 15 kV. A variety of natural and man-made external calibration standards were used for EPMA. Peak and background counting times were adjusted to 40 seconds for all elements. Replicate analyses on standard materials showed variation of <1%. The crystal structure of the spray deposited film was obtained by analysis of the corresponding X-ray diffraction (XRD) pattern, recorded by Bruker D8 advance diffractometer. Raman spectroscopy analysis was conducted with a micro Raman spectrometer (Renishaw system) in backscattering configuration using a diode-pumped solid-state laser at 532 nm with excitation power of 1 mW. Current density−voltage ($J-V$) characteristics of the final devices were obtained with an AM1.5G solar simulator (VS-0852) equipped with a 500 W xenon lamp and a Keithley sourcemeter (2612A, dual sourcemeter, 200 V). The light intensity of the solar simulator was calibrated with a Si photodiode (Fraunhofer) to 100 mW/cm^2. The quantum efficiency measurement was conducted with a PVE300 photovoltaic devices characterization system (Bentham) equipped with a xenon/quartz halogen light source and calibrated with Si/Ge reference detectors.

RESULTS AND DISCUSSION

Gradual Heating and Spray Process to Prevent Mo Oxidation. As Mo oxidized readily following eq 1, the selected prevention methodology would be to form a barrier layer around Mo to isolate it from oxygen in ambient environment. Options of barrier layer could be a thin MoS_2 film or CIS precursor itself. MoS_2 was commonly formed during

dx.doi.org/10.1021/am500317m | ACS Appl. Mater. Interfaces 2014, 6, 6638−6643

sulfurization of CIS films, whereas the metallic precursor film, which will eventually form a CIS film, was another viable alternative. The proposed chemical equations on formation of MoS_2 or CIS film are shown in eqs 3 and 4, respectively.[27] Thiourea reduces Cu^{2+} ions to Cu^{+} during the mixing of the aqueous precursor solutions and it also serves as a sulfur source for the formation of CIS. Cyanamide (H_2NCN) that was formed as a reaction product would probably react with water or oxygen during the pyrolysis process and removed as volatile compounds.[28]

$$Mo(s) + O_2(g) \rightarrow MoO_2(s) \quad (1)$$

with $\Delta H^{\circ}_{298}/R = -70\,700 \pm 250$ K[29]

$$SC(NH_2)_2(s) + OH^-(aq) \rightarrow SH^-(aq) + H_2NCN(l) + H_2O \quad (2)$$

$$MoO_2(s) + 2SH^-(aq) \rightarrow MoS_2(s) + 2OH^-(aq) \quad (3)$$

$$2SH^-(aq) + Cu^+(aq) + In^{3+}(aq) + 2Cl^-(aq) \rightarrow CuInS_2(s) + 2HCl(g) \quad (4)$$

Glancing angle X-ray diffraction (GAXRD) with incidence angle of 1.0° was used to characterize the film at three different points of spray (Figure 1). The samples was extracted after 5 min of spray pyrolysis at temperature around 120-150°C (Initial phase). Only Mo peak (JCPDS card no. 42-1120) was observed at this initial phase as the deposition temperature of 120−150°C was too low to initiate reaction between precursor solutions. This resulted in the formation of a thin compact film (<100 nm) of precursor materials which completely covered the surface of the substrate, acting as a barrier layer protecting Mo surface from oxygen in the ambient. Low intensity CIS peak (JCPDS no. 85-1575) could be observed at the Intermediate phase after 10 min of spray pyrolysis at temperature around 200-250°C. During this phase, the temperature was sufficient for the precursors to react to form polycrystalline CIS film with a high degree of structural disorder. In addition, the dense CIS film formed would be sufficiently thick to prevent any oxygen from reaching the Mo surface. However, the wide FWHM (full width half maximum) and low intensity of the XRD peaks showed that the crystallinity and crystallite size were still poor (Scherrer's equation[30]). Peak intensity improvement, which could be an indication of crystallization, was observed at the end phase as higher substrate temperature of 300−350°C was used. To understand the importance of substrate heating, we analyzed XRD pattern of control sample deposited on preheated substrate (purple pattern in Figure 1). A shoulder peak 2θ = 26.5° was observed at the end phase of both samples (gradual heated substrate and preheated substrate). It could be β-In_2S_3 phase as the final film is Cu poor (Cu/In=0.85). This was also observed in spray deposited CIS on glass whereby Cu/In ratio is 1.0 and 0.8.[12,31,32] XRD patterns also indicated the absence of other binary compounds such as Cu_xS in the film. With a carefully controlled gradual heating and spray process, MoO_2 peak at 2θ = 36.9° (JCPDS card no. 32-0671) was not observed unlike the case of the CIS deposition on preheated Mo (purple pattern, Figure 1). To confirm that MoO_2 is formed when the Mo substrate were heated directly to the final spray temperature, we preheated the substrate to the intended final spray temperature without using any precursors and analyzed the XRD. MoO_2 formation could be observed during the preheating stage from the change in Mo texture and color which was also verified by XRD (Figure 1). EDX analysis revealed a higher atomic percentage of oxygen for CIS film deposited on preheated Mo (control sample) (14 ± 1 at %) as compared to the gradually heated Mo (6 ± 1 at %). Part of the oxygen detected originates from the soda-lime glass substrate.

Images a and b in Figure 2 show the cross-sectional SEM images of the films deposited on preheated Mo (control sample) and gradually heated Mo, showing an average grain

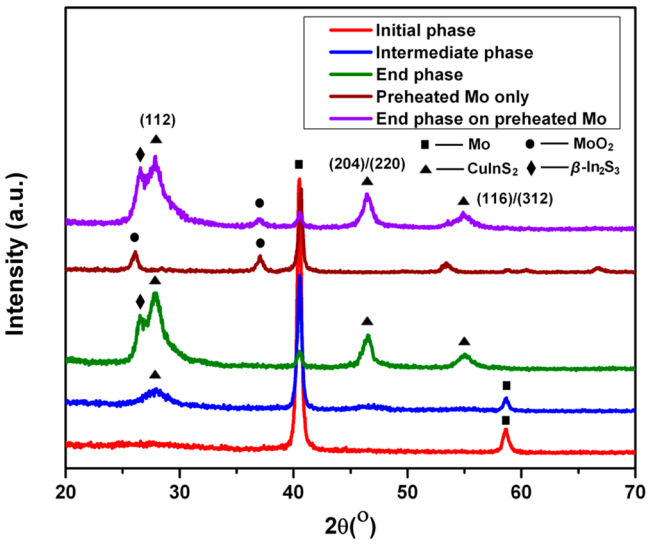

Figure 1. XRD patterns of the sprayed CIS films at different phases of deposition.

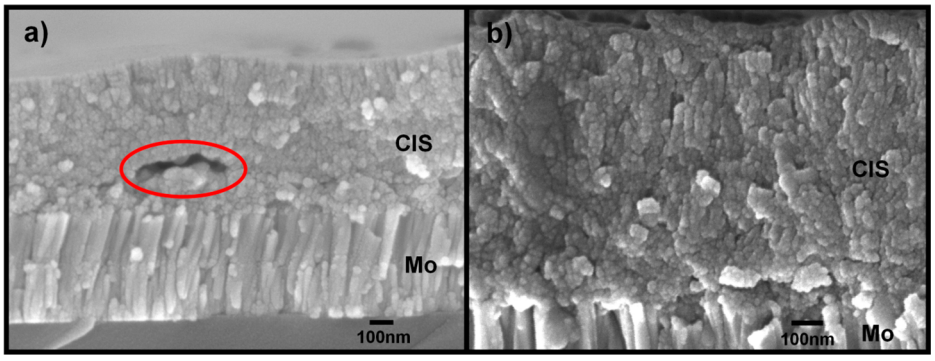

Figure 2. Cross-sectional SEM images of spray deposited CIS film deposited on (a) preheated Mo and (b) gradually heated Mo.

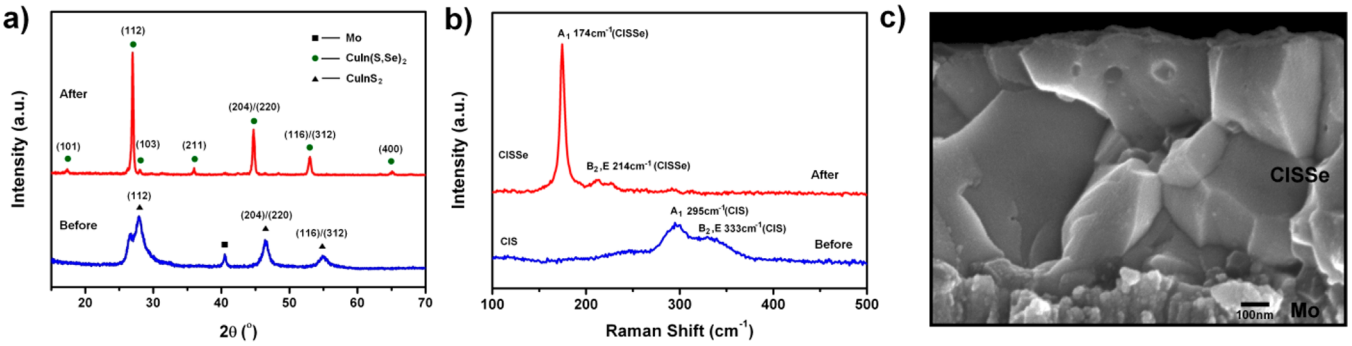

Figure 3. (a) XRD and (b) Raman spectra of CIS (blue, before selenization) and CISSe (red, after selenization) and (c) cross-sectional SEM image of spray deposited sample (I + II + III) after selenization at 480−500 °C for 10 min.

size of 15 nm. A thinner and less uniform film was obtained for the control sample (Figure 2a), possibly because of the formation of MoO_2, which reduces the wettability of water on the Mo surface. In addition, numerous pores similar to the one circled in Figure 2a were observed and usually formed near CIS/Mo interface. Unlike the film deposited on preheated Mo, the gradual heating and spray process resulted in a dense and more uniform film, which is more ideal for photovoltaic device application. We postulate that the slow ramp facilitates slower evaporation of solvent, which resulted in more dense CIS film and better adhesion with Mo.

Selenization and Characterization of CISSe. During the selenization step to induce grain growth, Se vapor was introduced by evaporation of Se pellet, a safer and easier alternative than the highly toxic H_2Se vapor. The partial substitution of S with Se in $CuInS_2$ to form $CuIn(S,Se)_2$ (CISSe) enables the tuning of the bandgap from 1.0 eV ($CuInSe_2$) to 1.5 eV ($CuInS_2$) depending on the selenization duration and amount of Se used, which affects the S/(S + Se) ratio. The bandgap adjustment via S/(S + Se) ratio tuning is similar to the effect of In/(In + Ga) ratio tuning in $Cu(In,Ga)Se_2$ (CIGS).[33] The selenization of all the films was conducted at 480-500°C for 10 min to observe grain growth and change in S/(S + Se) ratio. The temperature range of 480−500 °C was used for selenization to avoid the formation of the thick $MoSe_2$ layer that often results in film delamination.

The XRD patterns of the selenized film (Figure 3a) showed CISSe chalcopyrite peaks only. The β-In_2S_3 phase reacted with the highly diffusive Cu atoms at high temperature to form CIS. The 2θ position of the (112) peak at 26.95° of the selenized sample is left-shifted as compared to the sample before selenization because of the Se substitution in the CIS lattice causing an increase in the lattice parameters. The narrower FWHM of the peaks also indicated a significant increase in the crystallite size, consistent with the features shown in SEM image in Figure 3c (grain size 400−700 nm). In addition, the XRD pattern of CISSe films does not reveal the presence of any binary phases (e.g., Cu_xSe) after selenization.

To check for possible binary compounds in the sprayed film, we performed Raman spectroscopy. The Raman spectrum of the sample before selenization (Figure 3b) shows the dominant A_1 peak (295 cm^{-1}) signature of CIS with an additional shoulder peak (333 cm^{-1}), which could be from the B_2, E mode of CIS. The Raman spectrum agrees well with past reports on Cu-poor CIS film.[31,32,34] Secondary binary phases such as CuS and Cu_2S were not observed by Raman confirming their absence. Because β-In_2S_3 have main Raman peaks at 244 and 306 cm^{-1}, they may overlap with B_2 and E mode of CIS.[35] The Raman spectrum of the selenized CISSe film has a main peak at 174 cm^{-1} and the B_2, E mode of CISSe at 214 cm^{-1}. The peak at 174 cm^{-1} is slightly offset from the peak observed at 175−176 cm^{-1} on CISSe film formed via hydrazine approach, possibly because of the different S/Se ratios.[36] The absence of the Raman peak at 260 cm^{-1} indicates the absence of the binary CuSe phase in the selenized film, in agreement with the XRD results.

The grain size of the post-selenized gradually heated and spray-pyrolyzed CISSe film (Figure 3c) is approximately 400−700 nm, which was a significant improvement compared to the film before selenization (Figure 2b). It should be noted that selenization of the CIS film on preheated Mo (control sample) did not result in significant grain growth or densification of the porous film (see the Supporting Information). A possible reason could be the formation of the MoO_2 layer with a smaller crystallite size (MoO_2: 26 ± 1 nm by Rietveld Refinement) than Mo (Mo: 41 ± 2 nm by Rietveld refinement) resulted in more nucleation sites which limits grain growth of CIS during selenization. Hence, preheating of Mo substrate before CIS film deposition is not suitable for device application. The grain growth mechanism in spray-pyrolyzed CIS film should be similar to a typical chalcopyrite CIGS films. During selenization, some CuS/Cu_2S phase in the CIS film would react with Se vapor forming $CuSe/Cu_2Se$. These $CuSe/Cu_2Se$ would in turn dissociate into stoichiometrically different $Cu_{2-x}Se$ phases and liquid, Se which potentially enhances the grain growth through liquid-phase sintering (solid CISSe crystallites merging into one) and/or liquid phase epitaxy ($CuSe/Cu_2Se$ liquid reacts with In).[37]

The EDX data does not reveal the presence of both oxygen and carbon in the selenized CISSe film by gradual heating and spray process. The lack of carbon signal was expected as neither organic solvent nor organic binder materials (except thiourea) were used in the spraying process. Thiourea decomposes relatively easily forming CO_2 during spray pyrolysis, rendering carbon-free films. Stoichiometry of CISSe films was verified by WDS analysis which showed an average Cu/In ratio of 0.85 ± 0.01, similar to the average ratio of the as-prepared stock solution (0.85). The selenized film was predominantly single phase $CuIn(S,Se)_2$ with a low S/(S + Se) of 0.23 ± 0.01 determined by WDS. The estimated bandgap based on the S/(S + Se) ratio was 1.15 eV, close to the CIGS bandgap,[38] which results in optimum absorption.

$CuIn(S,Se)_2$ Device Characterization. The highest PCE (η) achieved from selenization of the gradual heating and spray-pyrolyzed CISSe device was 5.9%. The other devices fabricated in the same batch yielded PCE in range of 5−6% (device

dx.doi.org/10.1021/am500317m | ACS Appl. Mater. Interfaces 2014, 6, 6638−6643

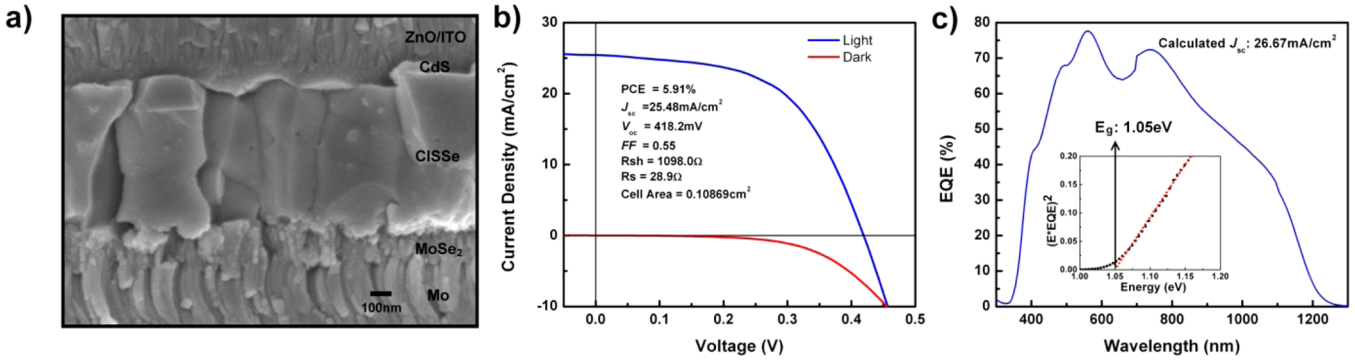

Figure 4. (a) Cross-sectional SEM image. (b) Current density−voltage (J−V) characteristics under AM1.5G (100 mW/cm^2) condition and (c) EQE curve of the CISSe device. Inset: Bandgap determination from EQE yielding 1.05 eV.

characteristics are provided in the Supporting Information). The best performance device was obtained by selenization of as deposited CIS film at 500°C for 30 min. A longer duration was selected to enhance grain growth and reduce S/(S + Se) ratio. The high efficiency achieved for spray-pyrolyzed absorber layer from precursor solution emphasizes great potential for low cost device fabrication. The current density-voltage (J−V) curve and device parameters are displayed in Fig. 4b (V_{oc} = 0.418 V, J_{sc} = 25.48 mA/cm^2, FF = 55.0%, and η = 5.9%). The V_{oc} of the device was still poor and could be attributed to the poor junction between the absorber layer and CdS. The J_{sc} was low as the absorber layer was relatively thin (700 nm, Figure 4a). The higher series resistance (28.9 Ω) may be attributed to the smaller grains (400−700 nm), which increases the probability of carrier recombination along grain boundaries. The series resistance issue could also be contributed by thicker CdS buffer layer, which was thicker than usual to ensure a more uniform coverage throughout the absorber layer. The higher resistance of ITO layer also contributed to the higher series resistance.

External quantum efficiency (EQE) spectrum of the corresponding device is shown in Fig. 4c. The bandgap estimate from EQE data was 1.05 eV, indicating a very low S/(S + Se) ratio. The effect of lower light absorption and higher series resistance on the device performance is also evident from the EQE data. The maximum EQE of around 78% is still significantly lower than that of the highest CISSe device reported (95%),[18] which could be attributed to low film thickness which was insufficient to absorb the light fully. There might also be more defect states and higher defect density in the CISSe film as the selenization condition could be optimized. The calculated J_{sc} from EQE data (26.67 mA/cm^2) is close to the measured J−V data (25.48 mA/cm^2). Future studies need to be done to optimize the selenization condition, film thickness, ITO layer, and S/(S + Se) ratio to achieve better photovoltaic performances.

CONCLUSION

Spray pyrolysis of device quality polycrystalline $CuInS_2$ (CIS) thin film on Mo substrate without oxidation by gradual heating and spray process was successfully demonstrated. Direct CIS deposition on preheated Mo would result in MoO_2 formation with some porosity and poor uniformity hence unsuitable for photovoltaic device application. Gradual heating process enables the formation of thin precursor film which acts as barrier layer protecting the Mo substrate. By using water as the solvent as well as increasing the amount of sulfur in the spray solution, carbon-free and oxygen-free CISSe thin film could be obtained after selenization. The best CISSe solar cell fabricated from the spray-pyrolyzed CIS absorber layer on Mo substrate yield a PCE of 5.9%. The simple spray method proposed here can be used to deposit a variety of Cu-based chalcopyrite precursor to produce high-quality thin film solar cell.

ASSOCIATED CONTENT

Supporting Information

Cross-sectional SEM image of CISSe films after selenization of $CuInS_2$ films spray deposited on preheated Mo substrate. WDS analysis of CISSe film to determine Cu/In and S/Se ratio. EDS data of CIS and CISSe films before and after selenization. I−V characteristics of CISSe solar cells. This material is available free of charge via the Internet at http://pubs.acs.org.

AUTHOR INFORMATION

Corresponding Author

*E-mail: LydiaWong@ntu.edu.sg.

Funding

Funding for this project is provided by A*STAR SERC Printed Photovoltaic Program (Grant No. 1021700143) and Singapore National Research Foundation (NRF) through the Singapore-Berkeley Research Initiative for Sustainable Energy (SinBeRISE) and Singapore National Research Foundation under CREATE programme: Nanomaterials for Energy and Water Management.

Notes

The authors declare no competing financial interest.

ACKNOWLEDGMENTS

The author (C.W.J.H.) thanks Economic Development Board (EDB) of Singapore for the scholarship. The authors thank Dr Jason Scott Herrin from the Facility for Analysis, Characterization, Testing, and Simulation (FACTS) at Nanyang Technological University (NTU) for the help on EPMA measurements; Lim Huimin for Raman measurements; and all the technical staffs from Energy Research Institute @ NTU (ERIAN) for support on lab facilities.

ABBREVIATIONS

CIS, $CuInS_2$
CISSe, $CuIn(S,Se)_2$
PCE, power conversion efficiency
SEM, scanning electron microscope
XRD, X-ray diffraction
WDS, wave dispersive spectroscopy

EDX, EDS, energy-dispersive spectroscopy

REFERENCES

(1) Repins, I.; Contreras, M. A.; Egaas, B.; DeHart, C.; Scharf, J.; Perkins, C. L.; To, B.; Noufi, R. 19·9%-Efficient ZnO/CdS/$CuInGaSe_2$ Solar Cell with 81·2% Fill Factor. *Prog. Photovoltaics Res. Appl.* **2008**, *16*, 235−239.

(2) Green, M. A.; Emery, K.; Hishikawa, Y.; Warta, W.; Dunlop, E. D. Solar Cell Efficiency Tables (version 43). *Prog. Photovoltaics Res. Appl.* **2014**, *22*, 1−9.

(3) Todorov, T. K.; Gunawan, O.; Gokmen, T.; Mitzi, D. B. Solution-Processed $Cu(In,Ga)(S,Se)_2$ Absorber Yielding a 15.2% Efficient Solar Cell. *Prog. Photovoltaics Res. Appl.* **2013**, *21*, 82−87.

(4) Guo, Q.; Ford, G. M.; Hillhouse, H. W.; Agrawal, R. Sulfide Nanocrystal Inks for Dense $Cu(In_{1-x}Ga_x)(S_{1-y}Se_y)_2$ Absorber Films and Their Photovoltaic Performance. *Nano Lett.* **2009**, *9*, 3060−3065.

(5) Akhavan, V. A.; Goodfellow, B. W.; Panthani, M. G.; Reid, D. K.; Hellebusch, D. J.; Adachi, T.; Korgel, B. A. Spray-Deposited $CuInSe_2$ Nanocrystal Photovoltaics. *Energy Environ. Sci.* **2010**, *3*, 1600−1606.

(6) Guo, Q.; Kim, S. J.; Kar, M.; Shafarman, W. N.; Birkmire, R. W.; Stach, E. A.; Agrawal, R.; Hillhouse, H. W. Development of $CuInSe_2$ Nanocrystal and Nanoring Inks for Low-Cost Solar Cells. *Nano Lett.* **2008**, *8*, 2982−2987.

(7) Wang, W.; Su, Y. W.; Chang, C. H. Inkjet Printed Chalcopyrite $CuIn_xGa_{1-x}Se_2$ Thin Film Solar Cells. *Sol. Energy Mater. Sol. Cells* **2011**, *95*, 2616−2620.

(8) Klugius, I.; Miller, R.; Quintilla, A.; Friedlmeier, T. M.; Blázquez-Sánchez, D.; Ahlswede, E.; Powalla, M. Growth Mechanism of Thermally Processed $Cu(In,Ga)S_2$ Precursors for Printed $Cu(In,Ga)(S,Se)_2$ Solar Cells. *Phys. Status Solidi RRL* **2012**, *6*, 297−299.

(9) Guo, Q.; Ford, G. M.; Agrawal, R.; Hillhouse, H. W. Ink Formulation and Low-Temperature Incorporation of Sodium to Yield 12% Efficient $Cu(In,Ga)(S,Se)_2$ Solar Cells from Sulfide Nanocrystal Inks. *Prog. Photovoltaics Res. Appl.* **2013**, *21*, 64−71.

(10) Jeong, S.; Lee, B.-S.; Ahn, S.; Yoon, K.; Seo, Y.-H.; Choi, Y.; Ryu, B.-H. An 8.2% Efficient Solution-Processed $CuInSe_2$ Solar Cell based on Multiphase $CuInSe_2$ Nanoparticles. *Energy Environ. Sci.* **2012**, *5*, 7539−7542.

(11) Kaelin, M.; Rudmann, D.; Tiwari, A. N. Low Cost Processing of CIGS Thin Film Solar Cells. *Sol. Energy* **2004**, *77*, 749−756.

(12) Krunks, M.; Kijatkina, O.; Rebane, H.; Oja, I.; Mikli, V.; Mere, A. Composition of $CuInS_2$ Thin Films Prepared by Spray Pyrolysis. *Thin Solid Films* **2002**, *403−404*, 71−75.

(13) Uhl, A. R.; Fella, C.; Chirilă, A.; Kaelin, M. R.; Karvonen, L.; Weidenkaff, A.; Borca, C. N.; Grolimund, D.; Romanyuk, Y. E.; Tiwari, A. N. Non-vacuum Deposition of $Cu(In,Ga)Se_2$ Absorber Layers from Binder Free, Alcohol Solutions. *Prog. Photovoltaics Res. Appl.* **2012**, *20*, 526−533.

(14) Ahn, S.; Son, T. H.; Cho, A.; Gwak, J.; Yun, J. H.; Shin, K.; Ahn, S. K.; Park, S. H.; Yoon, K. $CuInSe_2$ Thin-Film Solar Cells with 7.72% Efficiency Prepared via Direct Coating of a Metal Salts/Alcohol-Based Precursor Solution. *ChemSusChem* **2012**, *5*, 1773−1777.

(15) Ahn, S.; Choi, Y. J.; Kim, K.; Eo, Y.-J.; Cho, A.; Gwak, J.; Yun, J. H.; Shin, K.; Ahn, S. K.; Yoon, K. Amorphous Cu−In−S Nanoparticles as Precursors for $CuInSe_2$ Thin-Film Solar Cells with a High Efficiency. *ChemSusChem* **2013**, *6*, 1282−1287.

(16) Ahn, S.; Kim, K.; Cho, A.; Gwak, J.; Yun, J. H.; Shin, K.; Ahn, S.; Yoon, K. CuInSe2 (CIS) Thin Films Prepared from Amorphous Cu−In−Se Nanoparticle Precursors for Solar Cell Application. *ACS Appl. Mater. Interfaces* **2012**, *4*, 1530−1536.

(17) Harvey, T. B.; Mori, I.; Stolle, C. J.; Bogart, T. D.; Ostrowski, D. P.; Glaz, M. S.; Du, J.; Pernik, D. R.; Akhavan, V. A.; Kesrouani, H.; Vanden Bout, D. A.; Korgel, B. A. Copper Indium Gallium Selenide (CIGS) Photovoltaic Devices Made Using Multistep Selenization of Nanocrystal Films. *ACS Appl. Mater. Interfaces* **2013**, *5*, 9134−9140.

(18) Liu, W.; Mitzi, D. B.; Yuan, M.; Kellock, A. J.; Chey, S. J.; Gunawan, O. 12% Efficiency $CuIn(Se,S)_2$ Photovoltaic Device Prepared Using a Hydrazine Solution Process. *Chem. Mater.* **2010**, *22*, 1010−1014.

(19) Mitzi, D. B.; Yuan, M.; Liu, W.; Kellock, A. J.; Chey, S. J.; Deline, V. R.; Schrott, A. G. A High-Efficiency Solution-Deposited Thin Film Photovoltaic Device. *Adv. Mater.* **2008**, *20*, 3657−3662.

(20) Mooney, J. B.; Radding, S. B. Spray Pyrolysis Processing. *Annu. Rev. Mater. Sci.* **1982**, *12*, 81−101.

(21) Pamplin, B.; Feigelson, R. S. Spray Pyrolysis of $CuInSe_2$ and Related Ternary Semiconducting Compounds. *Thin Solid Films* **1978**, *60*, 141−146.

(22) Bates, C. W.; Nelson, K. F.; Raza, S. A. Spray Pyrolysis and Heat Treatment of $CuInSe_2$ for Photovoltaic Applications. *Thin Solid Films* **1982**, *88*, 279−283.

(23) Tomar, M. S.; Garcia, F. J. A ZnO/p-$CuInSe_2$ Thin Film Solar Cell Prepared Entirely by Spray Pyrolysis. *Thin Solid Films* **1982**, *90*, 419−423.

(24) Ahn, S.; Kim, K. H.; Yun, J. H.; Yoon, K. H. Effects of Selenization Conditions on Densification of $Cu(In,Ga)Se_2$ (CIGS) Thin Films Prepared by Spray Deposition of CIGS Nanoparticles. *J. Appl. Phys.* **2009**, *105*, 113533−7.

(25) Cai, Y.; Ho, J. C. W.; Batabyal, S. K.; Liu, W.; Sun, Y.; Mhaisalkar, S. G.; Wong, L. H. Nanoparticle-Induced Grain Growth of Carbon-Free Solution-Processed $CuIn(S,Se)_2$ Solar Cell with 6% Efficiency. *ACS Appl. Mater. Interfaces* **2013**, *5*, 1533−1537.

(26) Mao, J.; Shu, Q.; Wen, Y.; Yuan, H.; Xiao, D.; Choi, M. M. F. Facile Fabrication of Porous CuS Nanotubes Using Well-Aligned $[Cu(tu)]Cl·1/2H_2O$ Nanowire Precursors as Self-Sacrificial Templates. *Cryst. Growth Des.* **2009**, *9*, 2546−2548.

(27) O'Brien, P.; McAleese, J. Developing an Understanding of the Processes Controlling the Chemical Bath Deposition of ZnS and CdS. *J. Mater. Chem.* **1998**, *8*, 2309−2314.

(28) Madarász, J.; Pokol, G. Comparative Evolved Gas Analyses on Thermal Degradation of Thiourea by Coupled TG-FTIR and TG/DTA-MS Instruments. *J. Therm. Anal. Calorim.* **2007**, *88*, 329−336.

(29) Brewer, L.; Lamoreaux, R. H. The Mo−O System (Molybdenum-Oxygen). *Bull. Alloy Phase Diagrams* **1980**, *1*, 85−89.

(30) Patterson, A. L. The Scherrer Formula for X-Ray Particle Size Determination. *Phys. Rev.* **1939**, *56*, 978−982.

(31) Oja, I.; Nanu, M.; Katerski, A.; Krunks, M.; Mere, A.; Raudoja, J.; Goossens, A. Crystal Quality Studies of $CuInS_2$ Films Prepared by Spray Pyrolysis. *Thin Solid Films* **2005**, *480-481*, 82−86.

(32) Lee, D.-Y.; Kim, J. Characterization of Sprayed $CuInS_2$ films by XRD and Raman Spectroscopy Measurements. *Thin Solid Films* **2010**, *518*, 6537−6541.

(33) Wei, S. H.; Zhang, S. B.; Zunger, A. Effects of Ga Addition to $CuInSe_2$ on its Electronic, Structural, and Defect Properties. *Appl. Phys. Lett.* **1998**, *72*, 3219−3201.

(34) Álvarez-García, J.; Marcos-Ruzafa, J.; Pérez-Rodríguez, A.; Romano-Rodríguez, A.; Morante, J. R.; Scheer, R. MicroRaman Scattering from Polycrystalline $CuInS_2$ Films: Structural Analysis. *Thin Solid Films* **2000**, *361-362*, 208−212.

(35) Kambas, K.; Spyridelis, J.; Balkanski, M. Far Infrared and Raman Optical Study of α- and β-In_2S_3 Compounds. *Phys. Status Solidi B* **1981**, *105*, 291−296.

(36) Chung, C.-H.; Bob, B.; Lei, B.; Li, S.-H.; Hou, W. W.; Yang, Y. Hydrazine Solution-Processed $CuIn(Se,S)_2$ Thin Film Solar Cells: Secondary Phases and Grain Structure. *Sol. Energy Mater. Sol. Cells* **2013**, *113*, 148−152.

(37) Albin, D.; Tuttle, J.; Noufi, R. The Formation of Large-Grain $CuInSe_2$ Films by Selenization by High-Rate Se Transport under Moderate Vacuum Conditions. *J. Electron. Mater.* **1995**, *24*, 351−357.

(38) Contreras, M. A.; Ramanathan, K.; AbuShama, J.; Hasoon, F.; Young, D. L.; Egaas, B.; Noufi, R. Diode Characteristics in State-Of-The-Art ZnO/CdS/$Cu(In_{1-x}Ga_x)Se_2$ Solar Cells. *Prog. Photovoltaics Res. Appl.* **2005**, *13*, 209−216.